



OPEN

Abrupt upwelling and CO₂ outgassing episodes in the north-eastern Arabian Sea since mid-Holocene

Syed Azharuddin^{1,4}, Pawan Govil^{1✉}, Thomas B. Chalk², Mayank Shekhar¹, Gavin L. Foster² & Ravi Mishra³

Identifying the causes and consequences of natural variations in ocean acidification and atmospheric CO₂ due to complex earth processes has been a major challenge for climate scientists in the past few decades. Recent developments in the boron isotope ($\delta^{11}\text{B}$) based seawater pH and pCO₂ (or pCO₂^{sw}) proxy have been pivotal in understanding the various oceanic processes involved in air-sea CO₂ exchange. Here we present the first foraminifera-based $\delta^{11}\text{B}$ record from the north-eastern Arabian Sea (NEAS) covering the mid-late Holocene (~8–1 ka). Our record suggests that the region was overall a moderate to strong CO₂ sink during the last 7.7 kyr. The region behaved as a significant CO₂ source during two short intervals around 5.5–4 ka and 2.8–2.5 ka. The decreased pH and increased CO₂ outgassing during those abrupt episodes are associated with the increased upwelling in the area. The upwelled waters may have increased the nutrient content of the surface water through either increased supply or weaker export production. This new dataset from the coastal NEAS suggests that, as a potential result of changes in the strength of the El-Nino Southern Oscillation, the region experienced short episodes of high CO₂ outgassing and pre-industrial ocean acidification comparable to or even greater than that experienced during the last ~200 years.

The recent rapid increase in anthropogenic CO₂ has led to ocean acidification negatively impacting marine carbonate ecosystems¹. The level of carbon dioxide (CO₂) in the atmosphere has a direct role in regulating the chemistry of the ocean. The dissolution of anthropogenic CO₂ in seawater has lowered ocean pH and carbonate ion concentrations and potentially reduced the ability of marine organisms to calcify². Pre-industrial variations in atmospheric CO₂ are believed to be strongly influenced by changes in circulation and carbon cycling in the ocean^{3–5} where the interaction between large deep ocean carbon reserves and dynamic ocean circulation plays an important role in regulating the ocean carbonate system and air-sea gas exchange of CO₂^{3,4}. The mechanism involved in this exchange of CO₂ consists of several complex processes which alter the magnitude of oceanic sinks (mainly cold, high latitude regions) and sources (mainly warm, low latitude and tropical regions)^{3,6,7}. The ocean carbonate system consists of six co-varying parameters (pH, [CO₂], [HCO₃⁻], [CO₃²⁻], total alkalinity (TA) and dissolved inorganic carbon (DIC)), with the full system resolvable provided any two of these six components are known. Moreover, surface water pH and pCO₂ are very tightly coupled in natural systems and thus knowledge of one is enough to infer the other with high confidence⁸. On a glacial-interglacial timescale, the processes influencing the concentration of CO₂ in the atmosphere are thought to leave a fingerprint on the surface water pH⁹. Also, the pH of the surface water is the primary control of the boron isotope composition in planktonic foraminifera^{10–14}. Therefore, the boron isotope signatures ($\delta^{11}\text{B}$) of planktonic foraminifera provides a good opportunity to better understand the changes in surface ocean chemistry (pH) and the mechanisms involved in regulating the ocean carbonate system before human influence and industrialization, as well as providing a way to produce reconstructions of past pH and atmospheric CO₂¹⁵.

The Arabian Sea is one of the most productive basins of the world, having the capability to release around 90 TgC yr⁻¹ to the atmosphere^{16,17}. The monsoon-influenced lateral and vertical circulation of nutrients in the

¹Birbal Sahni Institute of Palaeosciences, 53 University Road, Lucknow, U.P. 226007, India. ²School of Ocean and Earth Science, National Oceanography Centre Southampton, University of Southampton Waterfront Campus, Southampton SO14 3ZH, UK. ³National Centre of Polar and Ocean Research, Headland Sada, Vasco-da-Gama, Goa 403 804, India. ⁴Present address: School of Earth and Environmental Sciences, Seoul National University, Gwanak-gu, Seoul 08826, South Korea. ✉email: pawan_govil@bsip.res.in

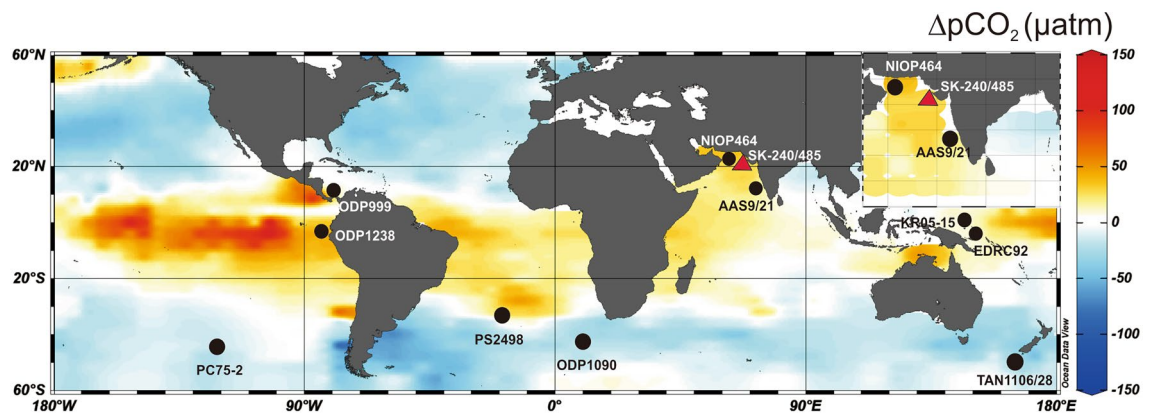


Figure 1. Map of modern sea surface $\Delta p\text{CO}_2$ distribution in the world ocean (60°N–60°S)²⁶ (<https://www.pmel.noaa.gov/co2/story/Surface+CO2+Flux+maps>). Red triangle shows the current study site SK-240/485 nearby offshore Saurashtra, north-eastern Arabian Sea. Black circles show the other boron isotope records referred to in this study. The inset figure shows $\Delta p\text{CO}_2$ distribution in the northern Indian Ocean. The Map was prepared using Ocean Data View (<http://www.odv.awi.de>)⁴⁰.

water column plays an important role in regulating the productivity of the basin¹⁸. The majority of the southern, western and central parts of Arabian Sea are characterised by high productivity during the summer season (during south-west monsoon or SWM), due to high riverine flux and SWM influenced upwelling^{19,20}. However, the northern and north-eastern parts of Arabian Sea experience comparatively high productivity during the winter season^{21,22}, this is due to the combined effect of northeast monsoon (NEM) influenced winter mixing^{23–25} as well as the nutrient-rich water advected from Bay of Bengal via the south-eastern Arabian Sea (West Indian Coastal Current or WICC).

Surface water $p\text{CO}_2$ (or $p\text{CO}_2^{\text{sw}}$) in the Arabian Sea is strongly influenced by physical, chemical, and biological processes which ultimately depend on the Indian Summer Monsoon and related sea surface circulation^{17,26,27}. The available palaeo- $p\text{CO}_2^{\text{sw}}$ records from Arabian Sea suggest that the north central sector (Site NIOP464 around Murray Ridge) was a consistent source of the CO_2 between 29 and 5 ka, whereas the south-eastern Arabian Sea (Site AAS9/21) is thought to be a significant CO_2 sink from 23 to 5 ka^{17,28} (Fig. 1). Interestingly, both studies point towards the strength of Southwest Monsoon (SWM) as the main driver of $p\text{CO}_2^{\text{sw}}$ variation in the Arabian Sea in the past. Modern studies from Arabian Sea show a significant role for regional oceanography and climate on $p\text{CO}_2^{\text{sw}}$ variation during pre-, post-, and inter-monsoon seasons²⁹. Studies from coastal regions suggest that the near shore waters tend to show much more short-term temporal and spatial $p\text{CO}_2^{\text{sw}}$ variations than the open ocean due to large input of terrestrial carbon and nutrients from rivers and ground waters^{30,31}. More specifically, the continental shelves are CO_2 sinks with increased pH, whereas nearshore ecosystems behave as a strong CO_2 sources with decreased pH³⁰. Studies from upwelling areas suggest that the coastal Arabian Sea, in general, has potential to behave as both a source and sink of carbon dioxide³². This is due to the supply of terrestrial fresh water input mixed with terrestrial detritus and nutrients (including C). On a short-term, such coastal areas show lower pH estimates than further offshore and behave as CO_2 source. However, on the longer term, the biologically fixed carbon is deposited with the sediments in the deeper parts, which make the region a CO_2 sink with relatively high pH³³. Studies focused on the interaction between surface layer $p\text{CO}_2$ and air-sea exchange suggest that overall the modern Arabian Sea is a weak CO_2 source having a potential to degas $\sim 460 \text{ mmol C/m}^2/\text{yr}$ ³⁴. However, studies related to the quantification of monsoon-controlled export flux to the interior parts of Arabian Sea suggests that the carbon-captured by sediments during upwelling is a potential sink of $\sim 820 \text{ mmol C/m}^2/\text{yr}$ ³⁵. By virtue of such air-sea interaction, several modelling studies suggest that the inter-annual SST variability in the Indian Ocean is linked to internal oceanic cycling as well as the external atmospheric forcing^{36–39}. However, these existing teleconnections are yet to be explored in past climate records.

Therefore, studying a sediment core from coastal Arabian Sea may provide new insights into the mechanism(s) of past air-sea interaction, related variations in $p\text{CO}_2^{\text{sw}}$ and surface water acidification, and their possible global teleconnection. Here we used the coupled analysis of $\delta^{11}\text{B}$ and Mg/Ca ratio in planktonic foraminifera (*Globigerinoides ruber sensu stricto* (white), hereafter *G. ruber*) in a marine sediment core SK-240/485 collected from continental shelf offshore Saurashtra, NE Arabian Sea (Fig. 1). This study provides insights into the past pH and $p\text{CO}_2^{\text{sw}}$, sea surface temperature (SST) and salinity (SSS) variations to understand the role of the monsoon and associated regional oceanographic settings in regulating the past air-sea interaction in the area during mid-late Holocene.

Results and discussion

The surface water above core SK-240/485, is strongly influenced by the SWM with very little contribution from the NEM^{41,42}, despite being located in the NE Arabian Sea. The SWM is considered as the major regulator of SST and SSS, particularly in coastal regions. This can also be observed in the monthly salinity record of nearby location (21.5°N; 68.5°E) which shows an extreme SSS decrease around October (post-SWM) (Supplementary Fig. 1). The surface-dwelling foraminifera *G. ruber* inhabits the upper water column (down to $\sim 25 \text{ m}$) when

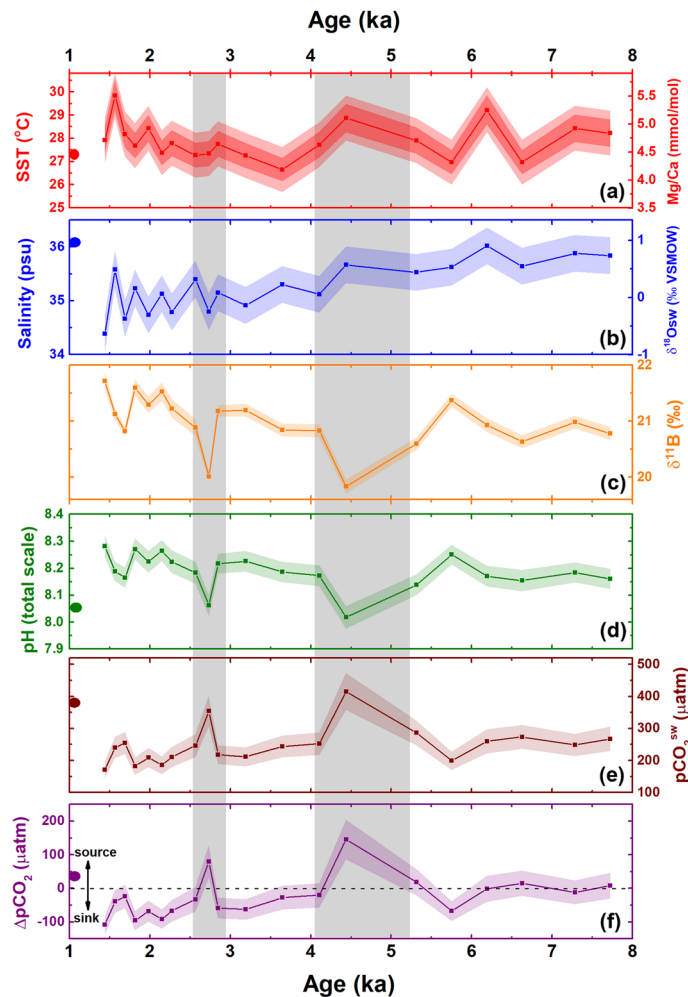


Figure 2. Down core variation of (a) Sea surface temperature (SST) (°C) and Mg/Ca ratio in *G. ruber* (mmol/mol) (b) Salinity (psu) and $\delta^{18}\text{O}_{\text{sw}}$ (‰ VSMOW) (c) $\delta^{11}\text{B}$ (‰) (d) pH (total scale) (e) pCO_2^{sw} (μatm) and (f) ΔpCO_2 ($\text{pCO}_2^{\text{sw}} - \text{pCO}_2^{\text{atm}}$) (μatm) in the core SK-240/485. Point at y-axis (left side) represents the modern (2000 AD) value around the core site. Shaded region around the curve represents 2SD error of the data. In panel (a) dark shade = 2SD error of Mg/Ca and light shade = 2SD error of SST. Vertical grey bands mark the abrupt CO_2 outgassing episodes.

the surface water is well stratified due to increased fresh water discharge in the basin during the SWM season. Therefore, the reconstructed signals from the *G. ruber* proxy may be biased towards the SWM season (JJAS)^{43–45}. The Mg/Ca ratio of *G. ruber* at SK-240/285 shows an average value of 4.70 mmol/mol ($n=20$) which corresponds to an average SST of 27.9°C in the area during mid-late Holocene (7.72–1.44 ka) (Fig. 2a). At present, the average annual SST in the region is 27.2°C with maximum (29.3°C) and minimum (24.3°C) recorded in June and February respectively (Supplementary Fig. 1). The SST recorded by core SK-240/485 ranges between a minimum of 26.7°C (around 3.65 ka) to a maximum of 29.7°C (around 1.56 ka), which shows an overall 3°C variation of SST during the last 7.7 kyr (Fig. 2a). Mg/Ca based SST records from other parts of Arabian Sea suggest 2–3 °C variation in SST during the Holocene^{46–50} (site specific details in Supplementary Table 1), which is similar to the alkenone-based SST records from northern Arabian Sea (offshore Pakistan) which show ~3°C variation in SST during the Holocene attributed to the effect of winter monsoon in the area^{51,52}.

The $\delta^{18}\text{O}_{\text{sw}}$ derived SSS in the core SK-240/485 varies between 36.0 and 34.4 psu and shows a freshening trend during mid-late Holocene (Fig. 2b). The $\delta^{18}\text{O}_{\text{sw}}$ has been extensively used as a proxy for SWM-influenced evaporation-precipitation budget in the northern Indian Ocean^{50,53}. The $\delta^{18}\text{O}_{\text{sw}}$ at our site varies between +0.93 and -0.70 ‰ (VSMOW), with most negative value observed during the late Holocene (after ~4 ka; Fig. 2b and Supplementary Fig. 2b). Such a lowering of $\delta^{18}\text{O}_{\text{sw}}$ suggests a significant decrease in the evaporation-precipitation budget of the area, perhaps due to an overall intensification of the SMW during 8–1 ka. A Mann–Kendall trend test reveals a significant increasing trend in $\delta^{18}\text{O}_{\text{sw}}$ over our study interval [$T=0.686$; p value (two tailed) < 0.0001] (Supplementary Fig. 2b). These observations thus point towards the increased intensification of SWM between 8 and 1 ka, as the major contribution of fresh water to the core site comes from the Indus River and small seasonal tributaries during the SWM. Previously, a $\delta^{18}\text{O}_{G.ruber}$ based statistical and spectral study from the same

site (SK-240/485) also suggested an intensifying SWM trend during the Holocene^{41,42}. In addition, it is in good agreement with other studies from eastern Arabian Sea during this interval^{54,55}.

The boron isotopic composition of the foraminifera ($\delta^{11}\text{B}$) shows an average value of 21.0‰ and ranges between 21.7‰ (at around 1.44 ka) and 19.8‰ (at around 4.44 ka; Fig. 2c). The reconstructed pH in the core SK-240/485 has an average value of 8.19 pH units for last ~7.7 kyr (Fig. 2d), which shows a good agreement with the existing pH records of the Holocene from the Pacific (~8.15 pH units), Atlantic (~8.16 pH units), and Indian (~8.22 pH units) Oceans^{9,27,28,56–58}. More specifically, the variation of pH in the core SK-240/485 ranges between 8.02 (around 4.44 ka) and 8.28 (around 1.44 ka; Fig. 2d). The Mann Kendall trend test suggests a significant increasing trend [$T = 0.386$; p -value (two tailed) < 0.028] in surface water pH since 7.7 ka (Supplementary Fig. 2a). The calculated average pCO_2^{sw} at the study site for last 7.7 kyr is 247 μatm which is ~22 μatm (or ppm) lower than the average atmospheric CO_2 value (around 269 ppm) obtained from EPICA Dome-C ice core record ($\text{pCO}_2^{\text{atm}}$) over the same period⁵⁹. The pCO_2^{sw} attains a maximum of 415 μatm at around 4.4 ka and minimum of 170 μatm at around 1.4 ka (Fig. 2e). While the average pCO_2^{sw} at the site SK-240/485 is considerably lower than the average Holocene pCO_2^{sw} values recorded in Atlantic and Pacific Ocean^{9,58,60}, it is significantly higher (~30 μatm) than that recorded at site AAS9/21 in the south-eastern Arabian Sea²⁸ since ~8 ka (247 μatm at SK-240/485 vs ~214 μatm at AAS9/21). A modelling-based study of the evolution of pCO_2^{sw} from the Arabian Sea suggests the existence of a strong north–south gradient in the Arabian Sea due to the seasonal sea surface circulation dynamics¹⁷. The south-eastern Arabian Sea shows comparatively lower pCO_2^{sw} due to the fresh water input from the Bay of Bengal through the West Indian Coastal Current (WICC) during the NEM⁴¹. On the contrary, the NE Arabian Sea (including the present site) does not receive fresh water input from the WICC and therefore shows comparatively higher pCO_2^{sw} during modern times^{41,55}.

For a better understanding of the source/sink nature and quantification of air-sea CO_2 exchange in the studied region, we calculated the ΔpCO_2 (the difference of pCO_2^{sw} and $\text{pCO}_2^{\text{atm}}$) at each time interval (Fig. 2f). The cross-plot between ΔpCO_2 and salinity at the site SK-240/485 shows a significant positive correlation ($r = 0.65$; $p < 0.01$; R squared = 0.41 with exclusion of two points of high ΔpCO_2 (which are probably related to intense upwelling, see below, Supplementary Fig. 3). This suggests that the SWM-influenced freshwater input plays a significant role in the ΔpCO_2 variation of the area in the absence of strong upwelling. We found that the area was an overall CO_2 sink during the last 7.7 kyrs with average $\Delta\text{pCO}_2^{\text{sw}}$ around –25 μatm (ranging between 170 and 415 μatm) which is a value characteristic of shelf regions³⁰. Between 7.7 and 6.1 ka, the region was in quasi-equilibrium with the atmosphere with respect to CO_2 ($\Delta\text{pCO}_2 < 10 \mu\text{atm}$).

The record shows two abrupt periods since 7.7 ka when the region behaved as a significant CO_2 source, ~5.4–4.1 ka and ~2.8–2.6 ka. During these periods, pCO_2^{sw} and ΔpCO_2 were as high as 415 μatm and 145 μatm , respectively and surface water shows a notable 0.25 units decline in pH. During the same intervals, the $\delta^{13}\text{C}_{\text{G.ruber}}$ ($\delta^{13}\text{C}_{\text{GR}}$) from the same site (SK-240/485) shows a decrease of 0.5‰ centred around 4.5 kyr⁴¹ (Supplementary Fig. 4). Hence, the excess CO_2 in the surface water we see at site SK-240/485 around ~4.4 ka may be a result of weaker export production and/or enhanced nutrient-rich water masses reaching to the sea surface (e.g. upwelling). A negative excursion in $\delta^{13}\text{C}_{\text{G.ruber}}$ associated with the increased pCO_2^{sw} due to increased upwelling of nutrient-rich water has also been observed in the south-eastern Arabian Sea during the Bølling–Ållerød (warm period)²⁸. A similar pace of pH decrease along with high amounts of CO_2 outgassing was also observed around site MD01-2416 in sub-polar North Pacific during the Bølling–Ållerød which shows the significant response of local upwelling on the pCO_2 outgassing⁶¹. Based on these previous findings, we suggest that the outgassing at ~4.4 ka at SK-240/485 may be due to the supply of respired photosynthetic products to the surface along with the upwelled water, which increased the DIC/alkalinity ratio and thereby lowered pH and increased surface water CO_2 ⁶¹. However, the increase in Mg/Ca SST at the same time may either be related to the near-surface habitat of *G. ruber* and upper water column stratification, rather than upwelling to the surface; the replacement of surface water currents from a lower pH and warmer region; or the influence of non-thermal effects on Mg/Ca⁶². This latter possibility is discussed in more detail in the next section.

Non-thermal influences on foraminiferal Mg/Ca. Several studies suggest that the foraminifera bound Mg/Ca may be impacted by other environmental variables than temperature known as non-thermal effects⁶², including salinity⁶³ or carbonate system parameters^{61,64,65}. These studies highlight that the local changes in sea-water pH may exert a significant bias on the planktonic foraminifera Mg/Ca which lessens its correspondence to sea surface temperature (SST)^{61,65}. Based on such observations, a correction protocol has been suggested for the non-thermal influence on planktonic foraminifera Mg/Ca using MgCarb package⁶². We compared the original data with MgCarb-adjusted results to check the effect of such influences in our Arabian Sea record (Fig. 3). As expected, for much of the record, the MgCarb-adjustment causes little variation. However, a difference in calculated SST of ~2°C is observed at 4.4 and 2.7 ka (Fig. 3) where the lowest pH is observed. Because SST has a more minor control on the calculated pH, the adjusted pH record is largely within error of the original record but with a difference of ~0.06 units during 4.4 and 2.7 ka, corresponding to a maximum difference of ~50 μatm in ΔpCO_2 (with the adjusted pCO_2 values always being lower). Nevertheless, this adjustment represents only a minor change in the overall pH and ΔpCO_2 trends and hence the main inferences of our results remain unchanged (Fig. 3). Additionally, the adjusted SST during the periods of abrupt drop in pH and high CO_2 outgassing (marked by dark grey bands in Fig. 3) further supports the increased upwelling in the area at 2.7 ka.

Teleconnection of Arabian Sea upwelling with the El-Nino Southern Oscillation. The upwelling of sub-surface waters plays an important role in controlling the CO_2 saturation of the ocean surface. During intense upwelling, the surface waters are higher in CO_2 saturation relative to the atmospheric CO_2 level, decreasing surface water pH and causing CO_2 to outgas. The modern Arabian Sea experiences intense upwelling due

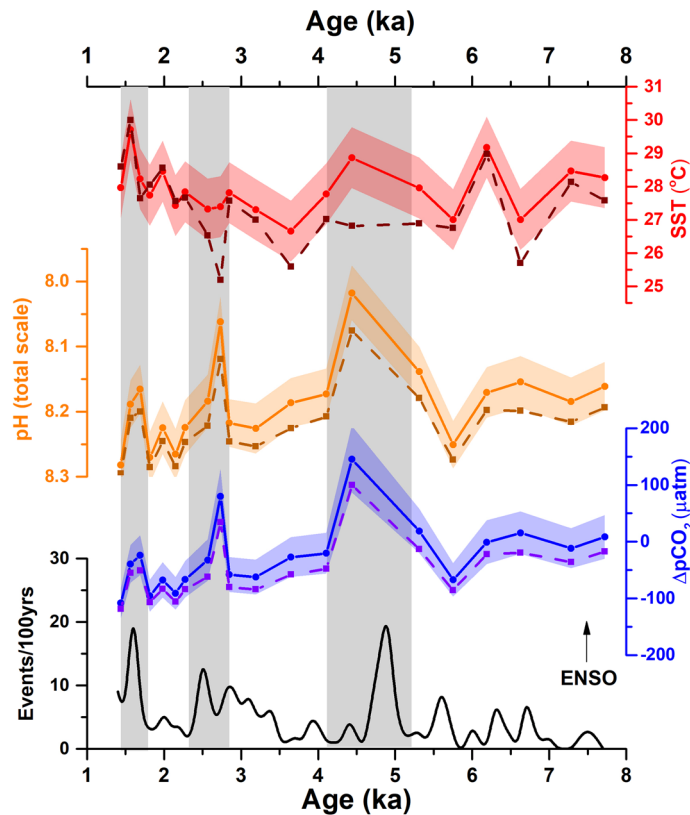


Figure 3. Comparison of original (solid lines) SST, pH and $\Delta p\text{CO}_2$ and nonthermal influence adjusted data (dashed lines) of site SK-240/485 with the frequency of ENSO events per 100 year⁶⁶. Shaded region around the curve represents 2SD error of the data. Vertical grey bands mark the abrupt variation in the proxy record.

to the action of southwest monsoon winds over the sea surface through Ekman pumping⁶⁷. Moreover, recent studies suggest a link between SWM and related upwelling in the Arabian Sea with the El Niño Southern Oscillation (ENSO)⁶⁸. In this context, we compared our record of pH and $\Delta p\text{CO}_2$ from site SK-240/485 with the proxy record of long-term ENSO activity during the Holocene (Figs. 3, 4): the variation of sedimentation around Laguna Palcacocha, South Ecuador that is thought to reflect the variation of ENSO activity in the area⁶⁶. The comparison reveals that the abrupt spikes in SST, $\Delta p\text{CO}_2$ and pH at 4.4 and 2.7 ka coincide with periods with high ENSO activity (Figs. 3, 4).

The ENSO is an important phenomenon of the tropical climate system. During positive ENSO phases basin-wide warming occurs throughout the tropical Indian Ocean⁶⁸, with several studies suggesting that SST variations in the Indian Ocean have a strong correlation with the ENSO variability^{71–74}. The Indian Ocean Basin Mode (IOBM) is the primary mode of variation of SST which has a strong impact on ENSO-induced heat-flux anomalies around Equatorial and northern Indian Ocean (including Arabian Sea)⁶⁸. During frequent ENSO events, the IOBM shows warming causing an increase in precipitation over tropical Indian Ocean and further strengthening the South Asian High⁶⁸. These climatic features influence the rising southwest monsoon winds over the Arabian Sea and result in the intensification of the Findlater Jet (FLJ)⁷⁵. In turn, the FLJ transports the moisture from the southern Indian Ocean to the Indian landmass through the Arabian Sea and inter-annual variation of FLJ has been linked to the strength of El Niño and La Niña episodes⁷⁶. The northward advancement of FLJ is reported to induce upwelling in the Arabian Sea^{76–78} and during an El Niño event the intensified FLJ advances towards the northern Arabian Sea where it induces strong coastal upwelling in the Arabian Sea via coastal Kelvin waves^{68,77,79–81}. These existing teleconnections are yet to be explored in records of past climate and are difficult to test, however, our observations suggest a strong influence of ENSO events on the upwelling around the NE Arabian Sea during mid-late Holocene, possibly similar to the modern-day relationship via coastal Kelvin waves. We therefore propose such a mechanism may have induced strong upwelling around the study area during the periods of high ENSO activity, increasing $\Delta p\text{CO}_2$ and surface water pH.

Comparison of global pre-industrial records with the modern analogue. For a better insight of our results in a global perspective, we have compared our $p\text{CO}_2^{\text{sw}}$ record with the existing records from Arabian Sea and other parts of the world ocean over the last 8–1 ka (Fig. 5 and Supplementary Table 2). We have also compared our results with global $p\text{CO}_2$ /pH composite curves prepared by considering several $\delta^{11}\text{B}$ based pH and $p\text{CO}_2^{\text{sw}}$ records to understand the behaviour of north-eastern Arabian Sea in context of global source/sink patterns⁶⁹ (See Supplementary Table 2 for more details). The $p\text{CO}_2$ records from equatorial and southwest Pacific

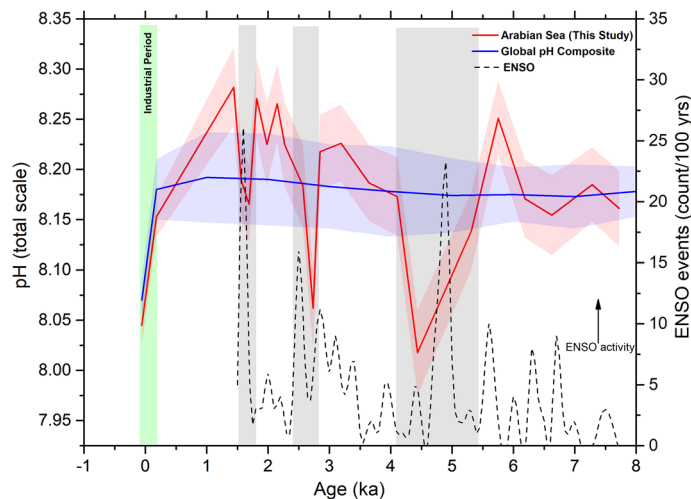


Figure 4. Comparison of Arabian Sea pH record around site SK-240/485 with the global pH composite⁶⁹ and ENSO events frequency/100 yr⁶⁶ since 8 ka. Vertical green band marks the industrial period. The modern (2010 AD) and pre-industrial (1770 AD) pH values (global and around site SK-240/485) are obtained from global ocean pH dataset⁷⁰. Shaded regions around the curve marks the uncertainty of the dataset. Vertical grey bands mark the abrupt drop in Arabian Sea pH during high ENSO activity.

Ocean (Sites ODP1238, EDRC-92 and PC 83-1) suggest that these areas were significant sources of CO₂ outgassing to the atmosphere during 8–1 ka^{58,60,69}. In contrast, a recent study from western equatorial Pacific region (Site KR05-15) indicates that the area is a modest CO₂ sink since the last glacial period⁸², whereas the eastern equatorial Pacific has continued to be a significant CO₂ source, the equatorial-western Pacific is currently in near equilibrium ($p\text{CO}_2^{\text{sw}} \approx p\text{CO}_2^{\text{atm}}$) and the south-western Pacific has changed to a modest sink of atmospheric CO₂ (Fig. 1)⁸³. The pCO₂^{sw} record from the ODP Site 999 in Caribbean Sea (Atlantic) indicates that the region was in near equilibrium ($p\text{CO}_2^{\text{sw}} \approx p\text{CO}_2^{\text{atm}}$) over the last 8 kyr and continues to remain this way to the present⁹. On the other hand, the site PS2498 in the south of Atlantic (~ Southern Ocean) appears as a larger CO₂ source ~ 8 ka and is currently a modest CO₂ sink during modern times⁵⁸. A recent study from site TAN1106/28 around offshore New Zealand in the sub-Antarctic Pacific shows high pCO₂^{sw} leading to the CO₂ outgassing from the region around 4 ka⁸⁴ and a similar increase in CO₂ outgassing potentially caused by enhanced upwelling of CO₂-rich deep waters around 4.5 ka, this has also been reported from site MD972106 in Atlantic sector of Sub Antarctic Zone⁸⁵. The change in the Southern Ocean from a significant CO₂ source (during the deglacial and into the Holocene) to a significant sink in modern times has been attributed to the resumption of Antarctic upwelling and northward advection of CO₂-rich waters via Ekman pumping^{58,86}.

The currently available $\delta^{11}\text{B}$ based records from Indian Ocean are restricted to the Arabian Sea^{27,28}. The $\Delta p\text{CO}_2$ record around site AAS9/21, albeit at low resolution, indicates that the south-eastern Arabian Sea was a significant sink during last ~ 8 kyr²⁸. The present study provides new information about the changes in carbonate system around the coastal NE Arabian Sea during 7.7–1.4 ka. The data shows an overall sink in the area along with the high CO₂ outgassing episodes in the area (as discussed in the previous sections). At the present time, the average $\Delta p\text{CO}_2$ and pH nearby site SK-240/485 is around 37 μatm and 8.04 units respectively^{26,70}. It is worth mentioning here that the recent (2010 AD) pH nearby site SK-240/485 (8.04) is 0.03 units lower than the average pH of global ocean in 2010 AD⁷⁰ (Fig. 4 and Supplementary Fig. 5). We have compared the pre-industrial (1770 AD) and modern (2010 AD) pH at our core site based on a recent study of global pre-industrial, modern and future pH estimates⁷⁰. The pre-industrial pH value (during 1770 AD or ~ 0.18 BP) nearby the study area is estimated to be 8.15 which was also 0.03 units lower than the average pH of the global ocean (~ 8.18) at that time⁷⁰. During industrialisation (between 1770 AD—present) the surface water pH around the study area varied at a similar pace to the global surface water pH (i.e. dropped ~ 0.15 pH units) due to the significant increase in global atmospheric CO₂ levels⁷⁰. Furthermore, with the current rate of pH change, it is estimated that the Arabian Sea, similar to the global ocean, may experience around 0.2–0.3 pH units drop in pH by 2100 if no attempt is made to mitigate emissions⁷⁰.

Conclusion

The present $\delta^{11}\text{B}$ based pH and pCO₂^{sw} results from the site SK-240/485 in NE Arabian Sea suggest that the region overall behaved as a net CO₂ sink during Mid-Late Holocene, which is a typical characteristic of a shelf region. In addition, the region was nearly in equilibrium with the atmosphere during 7.7–6.1 ka. Thereafter, the area behaved as an abrupt CO₂ source during two short periods of strong ENSO activity during 5.5–4 ka (very strong CO₂ source) and 2.8–2.5 ka (moderate CO₂ source). The periods of abrupt increase in $\Delta p\text{CO}_2$ are likely associated with the enhanced upwelling of nutrient-rich waters to the surface. It is estimated that the two intense upwelling episodes (centring around 4.4 and 2.7 ka) triggered CO₂ outgassing and preindustrial ocean acidification similar to the modern levels. Subsequently, during 2.5–1.4 ka, the region behaved as a strong CO₂ sink probably due to the absence of upwelling. We suggest therefore that there is evidence of intense natural ocean

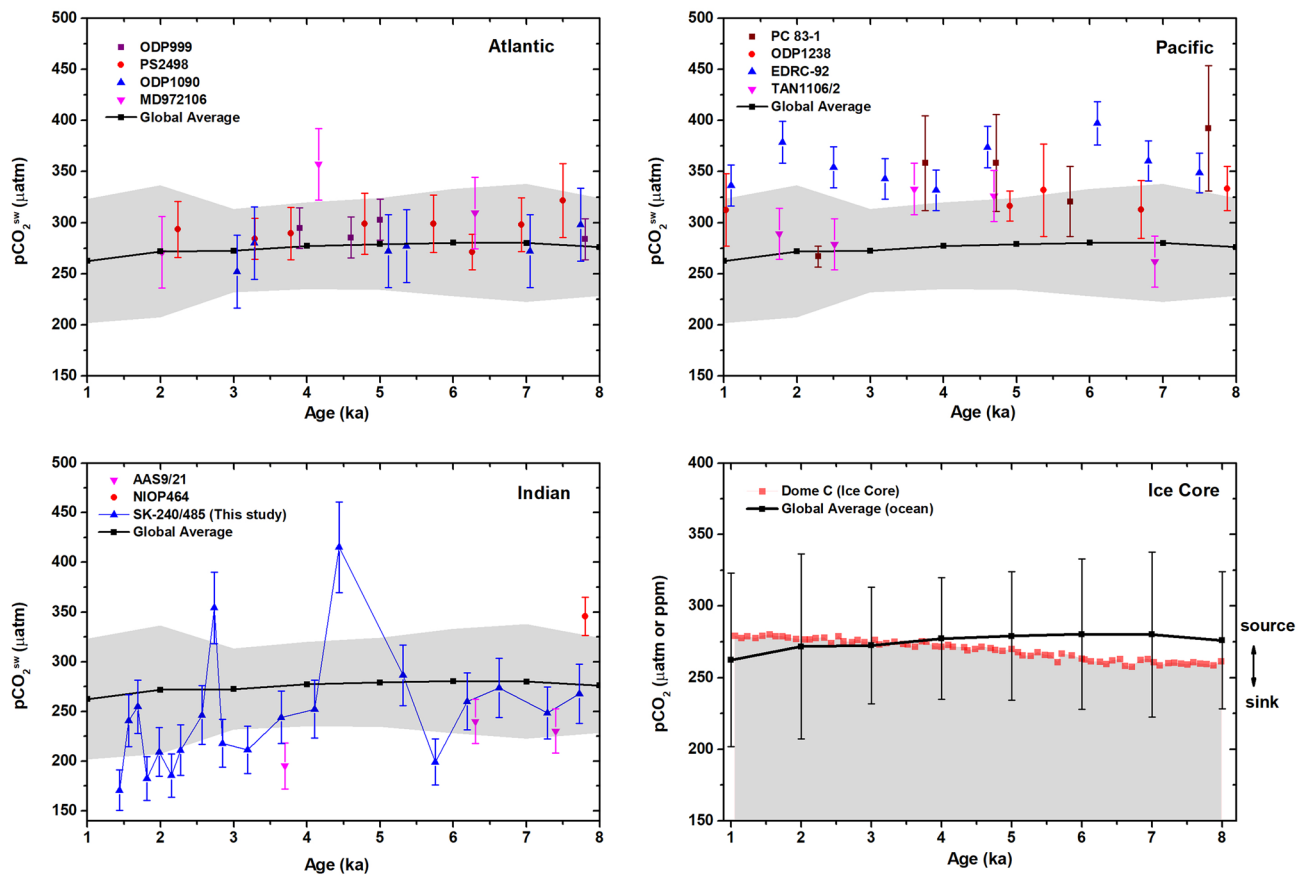


Figure 5. Comparison of published $p\text{CO}_2^{\text{sw}}$ results from Atlantic, Pacific and Indian Oceans and Dome C Ice Core with the global $p\text{CO}_2^{\text{sw}}$ composite⁶⁹ during 8–1 ka. Gray shaded in Atlantic, Pacific and Indian Ocean panels mark the uncertainty of global $p\text{CO}_2$ composite. Gray shaded region in the Ice Core panel indicates the sink. Refer text for more details.

acidification episodes in the region over the past at times of sudden increase in carbon and nutrient supply to the surface due to increased coastal upwelling. We found that the reconstructed pH from site SK-240/2485, as well as the pre-industrial and modern value, appears to be in the range of global pH variation during the Holocene (within uncertainty) except during these two abrupt periods of intense upwelling. A comparison of our data with available records of past ENSO activity suggests a possible teleconnection of NE Arabian Sea upwelling with the timing and intensity of ENSO events during the Holocene. However, this aspect in particular needs to be confirmed in future studies from other regions of the northern Indian Ocean.

Methods

Study area. The analysed marine sediment core (SK-240/485) was recovered from offshore Saurashtra (Lat. $21^\circ 16'$; Long. $68^\circ 55.99' \text{E}$; 88 m water depth), NE Arabian Sea (Fig. 1). The core covers time between the Pleistocene-Holocene boundary and the Holocene⁴² (last 12.4 kyr). However, the present study is restricted to cover the period between ~ 7.7 and ~ 1.4 ka due to insufficient foraminiferal abundance towards the bottom of the core.

The Arabian Sea is the north-western extension of Indian Ocean. It spreads around the coasts of India, Pakistan, Yemen, Oman, Somalia and the Addu Atoll (Maldives). The Indus River is the primary source of freshwater and sediment deposition in the NE Arabian Sea which receives fluxes of meltwater discharge from the Himalaya as well as runoff from monsoon precipitation^{87–89}. The Indus Fan is the most extensive physiographic feature of the Arabian Sea and considered to be the second-largest submarine fan in the world⁸⁹. Apart from the primary source, minor freshwater input also comes from the Bhadar River (a seasonal river) during the SWM season. The average annual salinity around the study area today is 36.2 psu, and the average annual sea surface temperature (SST) and $\Delta p\text{CO}_2$ (the difference between $p\text{CO}_2^{\text{sw}}$ and atmosphere) are 27.1°C and $+36.7 \mu\text{atm}$ respectively^{26,90} (Supplementary Fig. 1) with the latter having an annual cycle of $\sim 18 \mu\text{atm}$.

Geochemical proxies for studying ocean carbonate system. We analysed Mg/Ca ratios and $\delta^{11}\text{B}$ in planktonic foraminifera (*G. ruber*). The ratio of Mg to Ca (or Mg/Ca ratio) in calcite (particularly foraminifera) serves as a proxy of past seawater temperature and has been extensively used in the world oceans^{62,91–96}. The boron isotopic composition, expressed as $\delta^{11}\text{B}$ (Eq. 1), of foraminifera is strongly influenced by the pH of the

surface water^{9–11,14}. Hence, the $\delta^{11}\text{B}$ of planktonic foraminiferal shells is used as a proxy to reconstruct the pH of surface seawater and further to decipher other parameters of the ocean carbonate system, most notably pCO_2^{sw} .

$$\delta^{11}\text{B}(\text{‰}) = \left(\frac{\frac{^{11}\text{B}}{^{10}\text{B}}(\text{sample})}{\frac{^{11}\text{B}}{^{10}\text{B}}(\text{standard})} - 1 \right) \times 1000 \quad (1)$$

The geochemical analyses of foraminifera (Mg/Ca ratio and $\delta^{11}\text{B}$) were carried out at the University of Southampton, UK. For determination of Mg/Ca as well as $\delta^{11}\text{B}$ for each sample 170 individuals of *Globigerinoides ruber* (white variety; sensu-stricto type) with a size range of 300 to 350 μm were hand separated. The hand-separated specimens were then cleaned following Barker et al.⁹⁷, without applying the reductive cleaning step. Briefly, a multi-step cleaning protocol was applied consisting of crushing the foraminifera shells, followed by the removal of clay, silicate and organic matter, and a weak acid leaching with final dissolution of the carbonates using 0.5 M HNO_3 as detailed in Foster et al.⁹⁸. A small aliquot (~7%) of the cleaned and dissolved sample was analyzed for Mg and Ca (and other elemental ratios) by inductively coupled plasma mass spectrometry⁹ (ICP-MS) following Henehan et al.⁹⁹ while the remaining sample was analyzed for $\delta^{11}\text{B}$ using Multi collector inductive coupled plasma mass spectrometry (MC-ICP-MS) following Foster⁹. External reproducibility of the MC-ICPMS $\delta^{11}\text{B}$ method (at 95% confidence, 2SD) is based upon repeat measurements of an in house carbonate standard and is a function of sample concentration this ranges from 0.4‰ to 0.2‰ for the samples presented here^{57,98,100}. Analytical precision for elemental ratios is determined at 95% confidence by the reproducibility of several in house standards and is <5% for all elements. Strict criteria are used to rule out clay contaminated results (samples with Al/Ca > 100 $\mu\text{mol/mol}$ removed). All samples are matrix matched to a gravimetrically determined standard, to eliminate Ca concentration effects on the ratios produced⁹⁹.

The measured Mg/Ca (mmol/mol) ratio were converted to SST ($^{\circ}\text{C}$) by using the calibration equation¹⁰¹

$$\text{SST} = \left(\frac{1}{0.09} \right) * \ln \left(\frac{\text{Mg/Ca}}{0.38} \right) \quad (2)$$

Further, $\delta^{18}\text{O}$ of seawater ($\delta^{18}\text{O}_{\text{sw}}$) was calculated by using the SST derived from Mg/Ca to deconvolve ice volume effect values⁹⁵ from $\delta^{18}\text{O}$ of *G. ruber* and following equation of Bemis et al.¹⁰²

$$\delta^{18}\text{O}_{\text{sw}} = 0.27 + \left(\frac{T - 16.5 + 4.8 * \delta^{18}\text{O}_{\text{calcite}}}{4.8} \right) \quad (3)$$

The Sea Surface Salinity (SSS) was then calculated by using $\delta^{18}\text{O}_{\text{sw}}$ -salinity relation for Arabian Sea suggested in equation¹⁰³.

$$\text{Salinity} = \left(\frac{\delta^{18}\text{O}_{\text{sw}} + 20}{0.57} \right) \quad (4)$$

The pH was calculated from the analysed $\delta^{11}\text{B}$ values using the species-specific calibration for *G. ruber* (300–350 μm size range) of Henehan et al.⁵⁷ (See Eqs. 1, 5).

$$\text{pH} = \text{pK}_B^* - \log \left(\frac{-\delta^{11}\text{B}_{\text{sw}} - (\delta^{11}\text{B}_{\text{borate}})}{\delta^{11}\text{B}_{\text{sw}} - 11 - 10 \text{K}_B (\delta^{11}\text{B}_{\text{borate}}) - 1000 (11 - 10 \text{K}_B - 1)} \right) \quad (5)$$

where pK_B^* is the dissociation constant for boric acid dissociation in the in-situ (temperature, salinity and pressure) conditions and calculated as per Dickson¹⁰⁴, $\delta^{11}\text{B}_{\text{sw}}$ is the isotopic composition of seawater having value 39.61‰¹⁰⁵. $11 - 10 \text{K}_B$ is the equilibrium constant for the two existing forms of boron in seawater i.e. borate and boric acid¹⁰⁶ having a value of 1.0272 ± 0.0006 ¹⁰⁷. Since the borate ion is predominantly incorporated into the foraminifera calcite⁹, the $\delta^{11}\text{B}_{\text{CaCO}_3}$ can be used to obtain the pH with the species and size specific (*G. ruber*) coefficients as estimated by Henehan et al.⁵⁷ (See Eq. 5)

$$\delta^{11}\text{B}_{\text{borate}} = \left(\frac{\delta^{11}\text{B}_{\text{CaCO}_3} - 8.87 \pm 1.52}{0.6 \pm 0.09} \right). \quad (6)$$

Further, the pCO_2^{sw} was calculated from pH (derived from $\delta^{11}\text{B}$), SST and SSS (derived from Mg/Ca ratio) and TA (calculated using modern day relationship between SSS and TA around the area using the Global Data Analysis Project data set)⁷⁰.

All the original data calculations are done with the R computer programming platform¹⁰⁸ (R Core Team 2014) using “seacarb” package, version 6.8¹⁰⁹. Foraminifera bound Mg/Ca may be impacted by non-thermal effects⁶² (e.g. Gray and Evans 2019) including salinity⁶³ or carbonate parameters⁶⁴. We explored the influence of carbonate parameters using the parametrisation using MgCarb package as mentioned in Ref⁶². The uncertainties were calculated using Monte Carlo approach (n = 10,000) with consideration of the uncertainty in all relevant input parameters (with 95% confidence level) $\delta^{11}\text{B} \pm 0.25\%$; Mg/Ca derived SST $\pm 1^{\circ}\text{C}$; SSS $\pm 1\text{psu}$; TA $\pm 50 \mu\text{mol/kg}$.

Received: 20 February 2021; Accepted: 17 February 2022

Published online: 09 March 2022

References

- Raven, J., Caldeira, K., Elderfield, H., Hoegh-Guldberg, O., Liss, P., Riebesell, U., Shepherd, J., Turley, C. & Watson, A. Ocean acidification due to increasing atmospheric carbon dioxide. *R. Soc. https://royalsociety.org/topicspolicy/publications/2005/ocean-acidification/* (2005)
- Paytan, A. & Hönisch, B. Ocean acidification-A paleo perspective. *Limnol. Oceanogr. e-Lect.* **6**(2), 1–49 (2016).
- Sigman, D. M. & Boyle, E. A. Glacial/interglacial variations in atmospheric carbon dioxide. *Nature* **407**(6806), 859–869 (2000).
- Ahn, J. & Brook, E. J. Atmospheric CO₂ and climate on millennial time scales during the last glacial period. *Science* **322**(5898), 83–85 (2008).
- Joos, F., Battaglia, G., Fischer, H., Jeltsch-Thömmes, A. & Schmitt, J. Marine N₂O emissions during a Younger Dryas-like event: The role of meridional overturning, tropical thermocline ventilation, and biological productivity. *Environ. Res. Lett.* **14**(7), 075007 (2019).
- Toggweiler, J. R., Russell, J. L. & Carson, S. R. Midlatitude westerlies, atmospheric CO₂, and climate change during the ice ages. *Paleoceanography* **21**(2), PA2005. <https://doi.org/10.1029/2005PA001154> (2006).
- Brovkin, V., Ganopolski, A., Archer, D., & Rahmstorf, S. Lowering of glacial atmospheric CO₂ in response to changes in oceanic circulation and marine biogeochemistry. *Paleoceanography* **22**(4), PA4202. <https://doi.org/10.1029/2006PA001380> (2007).
- Hain, M. P., Foster, G. L. & Chalk, T. Robust constraints on past CO₂ climate forcing from the boron isotope proxy. *Paleoceanogr. Paleoclimatol.* **33**(10), 1099–1115 (2018).
- Foster, G. L. Seawater pH, pCO_{2sw} and [CO₃²⁻] variations in the Caribbean Sea over the last 130 kyr: A boron isotope and B/Ca study of planktic foraminifera. *Earth Planet. Sci. Lett.* **271**(1–4), 254–266 (2008).
- Hemming, N. G. & Hanson, G. N. Boron isotopic composition and concentration in modern marine carbonates. *Geochim. Cosmochim. Acta* **56**(1), 537–543 (1992).
- Sanyal, A., Nugent, M., Reeder, R. J. & Bijma, J. Seawater pH control on the boron isotopic composition of calcite: Evidence from inorganic calcite precipitation experiments. *Geochim. Cosmochim. Acta* **64**(9), 1551–1555 (2000).
- Hönisch, B. & Hemming, N. G. Surface ocean pH response to variations in pCO_{2sw} through two full glacial cycles. *Earth Planet. Sci. Lett.* **236**(1–2), 305–314 (2005).
- Pagani, M., Lemarchand, D., Spivack, A. & Gaillardet, J. A critical evaluation of the boron isotope-pH proxy: The accuracy of ancient ocean pH estimates. *Geochim. Cosmochim. Acta* **69**(4), 953–961 (2005).
- Foster, G. L. & Rae, J. W. Reconstructing ocean pH with boron isotopes in foraminifera. *Annu. Rev. Earth Planet. Sci.* **44**, 207–237 (2016).
- Foster, G. L. & Sexton, P. F. Enhanced carbon dioxide outgassing from the eastern equatorial Atlantic during the last glacial. *Geology* **42**(11), 1003–1006 (2014).
- Sharma, M., Papanastassiou, D. A. & Wasserburg, G. J. The concentration and isotopic composition of osmium in the oceans. *Geochim. Cosmochim. Acta* **61**(16), 3287–3299 (1997).
- Sarma, V. V. S. S. Monthly variability in surface pCO_{2sw} and net air sea CO₂ flux in the Arabian Sea. *J. Geophys. Res. Oceans*. **108**(C8), 11-1–11-13. <https://doi.org/10.1029/2001JC001062> (2003).
- Ryther, J. H. & Menzel, D. W. On the production, composition, and distribution of organic matter in the Western Arabian Sea. In *Deep Sea Research and Oceanographic Abstracts*, Vol. 12, No. 2, 199–209. (Elsevier, 1965). [https://doi.org/10.1016/0011-7471\(65\)90025-2](https://doi.org/10.1016/0011-7471(65)90025-2)
- Broerse, A. T. C., Brummer, G. J. & Van Hinte, J. E. Coccolithophore export production in response to monsoonal upwelling off Somalia (northwestern Indian Ocean). *Deep Sea Res. Part II* **47**(9–11), 2179–2205 (2000).
- Wakeham, S. G., Peterson, M. L., Hedges, J. I. & Lee, C. Lipid biomarker fluxes in the Arabian Sea, with a comparison to the equatorial Pacific Ocean. *Deep Sea Res. Part II* **49**(12), 2265–2301 (2002).
- Madhupratap, M. *et al.* Mechanism of the biological response to winter cooling in the northeastern Arabian Sea. *Nature* **384**(6609), 549–552 (1996).
- Goes, J. I. *et al.* Satellite and ship studies of phytoplankton along the west coast of India. In *Oceanography of the Indian Ocean* (ed. Desai, B. N.) 67–80 (Oxford & IBH Publishing Co, 1992).
- Andruleit, H. A., von Rad, U., Brans, A. & Ittekkot, V. Coccolithophore fluxes from sediment traps in the northeastern Arabian Sea off Pakistan. *Mar. Micropaleontol.* **38**(3–4), 285–308 (2000).
- Schulz, H., von Rad, U. & Ittekkot, V. Planktic foraminifera, particle flux and oceanic productivity off Pakistan, NE Arabian Sea: Modern analogues and application to the palaeoclimatic record. *Geol. Soc. Lond. Spec. Publ.* **195**(1), 499–516 (2002).
- Matondkar, S. P., Dwivedi, R. M., Parab, S., Pednekar, S., Desa, E. S., Mascarenhas, A. A. M. Q., Raman, M. & Singh, S. K. Satellite and ship studies of phytoplankton in the northeastern Arabian during 2000–2006 period. In *Remote Sensing of the Marine Environment*, Vol. 6406, 64061I. (International Society for Optics and Photonics, 2006).
- Takahashi, T. *et al.* Climatological mean and decadal change in surface ocean pCO₂, and net sea-air CO₂ flux over the global oceans. *Deep Sea Res. Part II Top. Stud. Oceanogr.* **56**(8–10), 554–577 (2009).
- Palmer, M. R. *et al.* Multi-proxy reconstruction of surface water pCO₂ in the northern Arabian Sea since 29 ka. *Earth Planet. Sci. Lett.* **295**(1–2), 49–57 (2010).
- Naik, S. S., Naidu, P. D., Foster, G. L. & Martínez-Botí, M. A. Tracing the strength of the southwest monsoon using boron isotopes in the eastern Arabian Sea. *Geophys. Res. Lett.* **42**(5), 1450–1458 (2015).
- Sarma, V. V. S. S., Kumar, M. D., Gauns, M. & Madhupratap, M. Seasonal controls on surface pCO₂ in the central and eastern Arabian Sea. *J. Earth Syst. Sci.* **109**(4), 471–479 (2000).
- Chen, C. T. A. & Borges, A. V. Reconciling opposing views on carbon cycling in the coastal ocean: Continental shelves as sinks and near-shore ecosystems as sources of atmospheric CO₂. *Deep Sea Res. Part II* **56**(8–10), 578–590 (2009).
- Chen, C. T. *et al.* Air–sea exchanges of CO₂ in the world's coastal seas. *Biogeosciences* **10**(10), 6509–6544 (2013).
- Smith, S. L. Understanding the Arabian Sea: Reflections on the 1994–1996 Arabian Sea expedition. *Deep Sea Res. Part II Top. Stud. Oceanogr.* **48**(6–7), 1385–1402 (2001).
- Watson, A. J. Are upwelling zones sources or sinks of CO₂? Upwelling in the ocean. *Mod. Process. Anc. Rec.* **18**, 321–336 (1995).
- Goyet, C., Gonçalves, R. I., & Touratier, F. Anthropogenic carbon distribution in the eastern South Pacific Ocean. *Biogeosciences* **6**(2) (2009).
- Honjo, S., Dymond, J., Prell, W. & Ittekkot, V. Monsoon-controlled export fluxes to the interior of the Arabian Sea. *Deep Sea Res. Part II* **46**(8–9), 1859–1902 (1999).
- Shukla, J. Effect of Arabian sea-surface temperature anomaly on Indian summer monsoon: A numerical experiment with the GFDL model. *J. Atmos. Sci.* **32**(3), 503–511 (1975).
- Shukla, J. Interannual variability of monsoons. *Monsoons* **14**, 399–464 (1987).
- Weare, B. C. A statistical study of the relationships between ocean surface temperatures and the Indian monsoon. *J. Atmos. Sci.* **36**(12), 2279–2291 (1979).
- Rao, K. G. & Goswami, B. N. Interannual variations of sea surface temperature over the Arabian Sea and the Indian monsoon: A new perspective. *Mon. Weather Rev.* **116**(3), 558–568 (1988).
- Schlitzer, R. Data analysis and visualization with Ocean Data View. *CMOS Bull. SCMO* **43**(1), 9–13 (2015).

41. Azharuddin, S. *et al.* Monsoon-influenced variations in productivity and lithogenic flux along offshore Saurashtra, NE Arabian Sea during the Holocene and Younger Dryas: A multi-proxy approach. *Palaeogeogr. Palaeoclimatol. Palaeoecol.* **483**, 136–146 (2017).
42. Azharuddin, S., Govil, P., Singh, A. D., Mishra, R. & Shekhar, M. Solar insolation driven periodicities in southwest monsoon and its impact on NE Arabian Sea paleoceanography. *Geosci. Front.* **10**(6), 2251–2263 (2019).
43. Be, A. W. An ecological, zoogeographic and taxonomic review of recent planktonic foraminifera. *Ocean. Micropaleontol.* **1**, 1–100 (1977).
44. Fairbanks, R. G., Wiebe, P. H. & Bé, A. W. Vertical distribution and isotopic composition of living planktonic foraminifera in the western North Atlantic. *Science* **207**(4426), 61–63 (1980).
45. Hilbrecht, H. Extant planktic foraminifera and the physical environment in the Atlantic and Indian Oceans: An atlas based on Climap and Levitus (1982) data. (1996).
46. Raza, T. *et al.* Glacial to Holocene changes in sea surface temperature and seawater $\delta^{18}\text{O}$ in the northern Indian Ocean. *Palaeogeogr. Palaeoclimatol. Palaeoecol.* **485**, 697–705 (2017).
47. Tiwari, M., Nagoji, S. S. & Ganeshran, R. S. Multi-centennial scale SST and Indian summer monsoon precipitation variability since the mid-Holocene and its nonlinear response to solar activity. *Holocene* **25**(9), 1415–1424 (2015).
48. Kessarkar, P. M., Purnachandra Rao, V., Naqvi, S. W. A. & Karapurkar, S. G. Variation in the Indian summer monsoon intensity during the Bølling Allerød and Holocene. *Paleoceanography* **28**(3), 413–425 (2013).
49. Saraswat, R., Lea, D. W., Nigam, R., Mackensen, A. & Naik, D. K. Deglaciation in the tropical Indian Ocean driven by interplay between the regional monsoon and global teleconnections. *Earth Planet Sci. Lett.* **375**, 166–175 (2013).
50. Govil, P. & Naidu, P. D. Evaporation-precipitation changes in the eastern Arabian Sea for the last 68 ka: Implications on monsoon variability. *Paleoceanography* **25**(1), PA1210. <https://doi.org/10.1029/2008PA001687> (2010).
51. Rolinski, S., Segsneider, J. & Sündermann, J. Long-term propagation of tailings from deep-sea mining under variable conditions by means of numerical simulations. *Deep Sea Res. Part II* **48**(17–18), 3469–3485 (2001).
52. Böll, A. *et al.* Contrasting sea surface temperature of summer and winter monsoon variability in the northern Arabian Sea over the last 25 ka. *Palaeogeogr. Palaeoclimatol. Palaeoecol.* **426**, 10–21 (2015).
53. Govil, P. & Naidu, P. D. Variations of Indian monsoon precipitation during the last 32 kyr reflected in the surface hydrography of the Western Bay of Bengal. *Quat Sci Rev.* **30**(27–28), 3871–3879 (2011).
54. Sarkar, A. *et al.* High resolution Holocene monsoon record from the eastern Arabian Sea. *Earth Planet. Sci. Lett.* **177**(3–4), 209–218 (2000).
55. Kumar, P. K. & Ramesh, R. Revisiting reconstructed Indian monsoon rainfall variations during the last ~ 25 ka from planktonic foraminiferal $\delta^{18}\text{O}$ from the Eastern Arabian Sea. *Quat. Int.* **443**, 29–38 (2017).
56. Yu, J., Elderfield, H., & Hönisch, B. B/Ca in planktonic foraminifera as a proxy for surface seawater pH. *Paleoceanography* **22**(2), PA2202. <https://doi.org/10.1029/2006PA001347> (2007)
57. Henehan, M. J. *et al.* Calibration of the boron isotope proxy in the planktonic foraminifera *Globigerinoides ruber* for use in palaeo-CO₂ reconstruction. *Earth Planet. Sci. Lett.* **364**, 111–122 (2013).
58. Martínez-Botí, M. A. *et al.* Boron isotope evidence for oceanic carbon dioxide leakage during the last deglaciation. *Nature* **518**(7538), 219–222 (2015).
59. Monnin, E. *et al.* Atmospheric CO₂ concentrations over the last glacial termination. *Science* **291**(5501), 112–114 (2001).
60. Palmer, M. R. & Pearson, P. N. A 23,000-year record of surface water pH and pCO₂ in the western equatorial Pacific Ocean. *Science* **300**(5618), 480–482 (2003).
61. Gray, W. R. *et al.* Deglacial upwelling, productivity and CO₂ outgassing in the North Pacific Ocean. *Nat. Geosci.* **11**(5), 340–344 (2018).
62. Gray, W. R. & Evans, D. Nothermal influences on Mg/Ca in planktonic foraminifera: A review of culture studies and application to the last glacial maximum. *Paleoceanogr. Paleoclimatol.* **34**(3), 306–315 (2019).
63. Nürnberg, D., Bijma, J. & Hemleben, C. Assessing the reliability of magnesium in foraminiferal calcite as a proxy for water mass temperatures. *Geochim. Cosmochim. Acta* **60**(5), 803–814 (1996).
64. Russell, A. D., Hönisch, B., Spero, H. J. & Lea, D. W. Effects of seawater carbonate ion concentration and temperature on shell U, Mg, and Sr in cultured planktonic foraminifera. *Geochim. Cosmochim. Acta* **68**(21), 4347–4361 (2004).
65. Evans, D., Wade, B. S., Henehan, M., Erez, J. & Müller, W. Revisiting carbonate chemistry controls on planktic foraminifera Mg/Ca: Implications for sea surface temperature and hydrology shifts over the Paleocene-Eocene thermal maximum and Eocene-Oligocene transition. *Clim. Past* **12**(4), 819–835 (2016).
66. Moy, C. M., Seltzer, G. O., Rodbell, D. T. & Anderson, D. M. Variability of El Niño/Southern Oscillation activity at millennial timescales during the Holocene epoch. *Nature* **420**(6912), 162–165 (2002).
67. Sirocko, F., Sarnthein, M., Lange, H. & Erlenkeuser, H. Atmospheric summer circulation and coastal upwelling in the Arabian Sea during the Holocene and the last glaciation. *Quatern. Res.* **36**(1), 72–93 (1991).
68. Yang, J., Liu, Q., Xie, S. P., Liu, Z., & Wu, L. Impact of the Indian Ocean SST basin mode on the Asian summer monsoon. *Geophys. Res. Lett.* **34**(2), L02708. <https://doi.org/10.1029/2006GL028571> (2007).
69. Shao, J. *et al.* Atmosphere-ocean CO₂ exchange across the last deglaciation from the Boron Isotope Proxy. *Paleoceanogr. Paleoclimatol.* **34**(10), 1650–1670 (2019).
70. Jiang, L. Q., Carter, B. R., Feely, R. A., Lauvset, S. K. & Olsen, A. Surface ocean pH and buffer capacity: Past, present and future. *Sci. Rep.* **9**(1), 1–11 (2019).
71. Klein, S. A., Soden, B. J. & Lau, N. C. Remote sea surface temperature variations during ENSO: Evidence for a tropical atmospheric bridge. *J. Clim.* **12**(4), 917–932 (1999).
72. Wolter, K. & Hastenrath, S. Annual cycle and long-term trends of circulation and climate variability over the tropical oceans. *J. Clim.* **2**(11), 1329–1351 (1989).
73. Krishnamurthy, V. & Kirtman, B. P. Variability of the Indian Ocean: Relation to monsoon and ENSO. *Q. J. R. Meteorol. Soc. J. Atmos. Sci. Appl. Meteorol. Phys. Oceanogr.* **129**(590), 1623–1646 (2003).
74. Dogar, M. M., Kucharski, F. & Azharuddin, S. Study of the global and regional climatic impacts of ENSO magnitude using SPEEDY AGCM. *J. Earth Syst. Sci.* **126**(2), 30 (2017).
75. Findlater, J. Mean monthly airflow at low levels over the western Indian Ocean. *Geophys. Memo.* **115**, 53 (1971).
76. Halpern, D. & Woiceshyn, P. M. Onset of the Somali jet in the Arabian Sea during June 1997. *J. Geophys. Res. Oceans* **104**(C8), 18041–18046 (1999).
77. Pushpanjali, B., Subrahmanyam, M. V., & Murty, K. V. (2014). Sea surface temperature and find later jet variations over Arabian Sea during summer monsoon. *J. Climatol. Weather Forecast.* **2**(2), 1000111. <https://doi.org/10.4172/2332-2594.1000111>.
78. Luther, M. E., O'Brien, J. J. & Prell, W. L. Variability in upwelling fields in the northwestern Indian Ocean I. Model experiments for the past 18,000 years. *Paleoceanography* **5**(3), 433–445 (1990).
79. Smitha, B. R., Sanjeevan, V. N., Vimalkumar, K. G. & Revichandran, C. On the upwelling off the southern tip and along the west coast of India. *J. Coastal Res.* **24**(10024), 95–102 (2008).
80. Rao, R. R. *et al.* Interannual variability of Kelvin wave propagation in the wave guides of the equatorial Indian Ocean, the coastal Bay of Bengal and the southeastern Arabian Sea during 1993–2006. *Deep Sea Res. Part I* **57**(1), 113 (2010).

81. Narvekar, J., Chowdhury, R. R., Gaonkar, D., Kumar, P. D. & Kumar, S. P. Observational evidence of stratification control of upwelling and pelagic fishery in the eastern Arabian Sea. *Sci. Rep.* **11**(1), 1–13 (2021).
82. Kubota, K. *et al.* Equatorial Pacific seawater pCO₂ variability since the last glacial period. *Sci. Rep.* **9**(1), 1–11 (2019).
83. Feely, R. A., Wanninkhof, R., Takahashi, T. & Tans, P. Influence of El Niño on the equatorial Pacific contribution to atmospheric CO₂ accumulation. *Nature* **398**(6728), 597–601 (1999).
84. Shuttlesworth, R. *et al.* Early deglacial CO₂ release from the Sub-Antarctic Atlantic and Pacific oceans. *Earth Planet. Sci. Lett.* **554**, 116649 (2021).
85. Moy, A. D. *et al.* Varied contribution of the Southern Ocean to deglacial atmospheric CO₂ rise. *Nat. Geosci.* **12**(12), 1006–1011 (2019).
86. Bostock, H. C. *et al.* The carbonate mineralogy and distribution of habitat-forming deep-sea corals in the southwest Pacific region. *Deep Sea Res. Part 1* **100**, 88–104 (2015).
87. Milliman, J. D., Qinchun, X. & Zuosheng, Y. Transfer of particulate organic carbon and nitrogen from the Yangtze River to the ocean. *Am. J. Sci.* **284**(7), 824–834 (1984).
88. Chauhan, O. S., Jayakumar, S., Menezes, A. A. A., Rajawat, A. S. & Nayak, S. R. Anomalous inland influx of the river Indus, Gulf of Kachchh, India. *Mar. Geol.* **229**(1–2), 91–100 (2006).
89. Miller, J. D., Immerzeel, W. W. & Rees, G. Climate change impacts on glacier hydrology and river discharge in the Hindu Kush-Himalayas. *Mt. Res. Dev.* **32**(4), 461–467 (2012).
90. Key, R. M. *et al.* A global ocean carbon climatology: Results from Global Data Analysis Project (GLODAP). *Glob. Biogeochem. Cycles*. **18**(4), GB4031. <https://doi.org/10.1029/2004GB002247> (2004).
91. Lea, D. W., Pak, D. K. & Spero, H. J. Climate impact of late Quaternary equatorial Pacific sea surface temperature variations. *Science* **289**(5485), 1719–1724 (2000).
92. Elderfield, H. & Ganssen, G. Past temperature and δ¹⁸O of surface ocean waters inferred from foraminiferal Mg/Ca ratios. *Nature* **405**(6785), 442–445 (2000).
93. Rosenthal, Y., Lohmann, G. P., Lohmann, K. C. & Sherrell, R. M. Incorporation and preservation of Mg in Globigerinoides sacculifer: Implications for reconstructing the temperature and ¹⁸O/¹⁶O of seawater. *Paleoceanography* **15**(1), 135–145 (2000).
94. Barker, S., Cacho, I., Benway, H. & Tachikawa, K. Planktonic foraminiferal Mg/Ca as a proxy for past oceanic temperatures: A methodological overview and data compilation for the Last Glacial Maximum. *Quat. Sci. Rev.* **24**(7–9), 821–834 (2005).
95. Saher, M. H., Peeters, F. J. C. & Kroon, D. Sea surface temperatures during the SW and NE monsoon seasons in the western Arabian Sea over the past 20,000 years. *Palaeogeogr. Palaeoclimatol. Palaeoecol.* **249**(1–2), 216–228 (2007).
96. Anand, P., Kroon, D., Singh, A. D., Ganeshram, R. S., Ganssen, G., & Elderfield, H. Coupled sea surface temperature–seawater δ¹⁸O reconstructions in the Arabian Sea at the millennial scale for the last 35 ka. *Paleoceanography* **23**(4), PA4207. <https://doi.org/10.1029/2007PA001564> (2008).
97. Barker, S., Greaves, M., & Elderfield, H. A study of cleaning procedures used for foraminiferal Mg/Ca paleothermometry. *Geochem. Geophys. Geosyst.* **4**(9), 8407(1–20). <https://doi.org/10.1029/2003GC000559> (2003).
98. Foster, G. L. & Rohling, E. J. Relationship between sea level and climate forcing by CO₂ on geological timescales. *Proc. Natl. Acad. Sci. United States*. **110**(4), 1209–1214 (2013).
99. Henehan, M. J. *et al.* Evaluating the utility of B/C a ratios in planktic foraminifera as a proxy for the carbonate system: A case study of *Globigerinoides ruber*. *Geochem. Geophys. Geosyst.* **16**(4), 1052–1069 (2015).
100. Rae, J. W., Foster, G. L., Schmidt, D. N. & Elliott, T. Boron isotopes and B/Ca in benthic foraminifera: Proxies for the deep ocean carbonate system. *Earth Planet. Sci. Lett.* **302**(3–4), 403–413 (2011).
101. Anand, P., Elderfield, H., & Conte, M. H. Calibration of Mg/Ca thermometry in planktonic foraminifera from a sediment trap time series. *Paleoceanography* **18**(2), 281–2815. <https://doi.org/10.1029/2002PA000846> (2003).
102. Bemis, B. E., Spero, H. J., Bijma, J. & Lea, D. W. Reevaluation of the oxygen isotopic composition of planktonic foraminifera: Experimental results and revised paleotemperature equations. *Paleoceanography* **13**(2), 150–160 (1998).
103. Dahl, K. A. & Oppo, D. W. Sea surface temperature pattern reconstructions in the Arabian Sea. *Paleoceanography* **21**(1), PA1014. <https://doi.org/10.1029/2005PA001162> (2006).
104. Dickson, A. G. Thermodynamics of the dissociation of boric acid in synthetic seawater from 273.15 to 318.15 K. *Deep Sea Res. Part A Oceanogr. Res. Pap.* **37**(5), 755–766 (1990).
105. Foster, G. L., Pogge von Strandmann, P. A. & Rae, J. W. B. Boron and magnesium isotopic composition of seawater. *Geochem. Geophys. Geosyst.* **11**(8), Q08015. <https://doi.org/10.1029/2010GC003201> (2010).
106. Zeebe, R. E., Sanyal, A., Ortiz, J. D. & Wolf-Gladrow, D. A. A theoretical study of the kinetics of the boric acid–borate equilibrium in seawater. *Mar. Geol.* **73**(2), 113–124 (2001).
107. Klochko, K., Kaufman, A. J., Yao, W., Byrne, R. H. & Tossell, J. A. Experimental measurement of boron isotope fractionation in seawater. *Earth Planet. Sci. Lett.* **248**(1–2), 276–285 (2006).
108. R Core Team R: A language and environment for statistical computing. R Foundation for Statistical Computing, Vienna, Austria. URL <https://www.R-project.org/> (2020).
109. Lavigne H., Epitalon, J. -M. & Gattuso J. -P. seacarb: Seawater carbonate chemistry with R. R package version 3.0. (2011). <http://CRAN.R-project.org/package=seacarb>

Acknowledgements

The authors are grateful to Director, BSIP, Lucknow and University of Southampton for providing necessary facilities to carry out this work and permitting us to publish the same. PG is thankful to the Foster Lab at UK for carrying out the analytical work of δ¹¹B and Mg/Ca. SA is also indebted for the award of Junior Research Fellowship under SERB-DST Project No. SR/FTP/ES-53/2013 and Senior Research Fellowship by the Council of Scientific and Industrial Research (CSIR-SRF Grant No. 09/528/0022/2018/EMR-5). Extended thanks to Prof Jinho Ahn, School of Earth and Environmental Sciences, Seoul National University, S. Korea and Dr Pyarimohan Maharana, Nalanda University, India for their valuable suggestions during the revision. This work was supported by fast-track Grant of SERB-DST under Project No. SR/FTP/ES-53/2013.

Author contributions

S.A.—Conceived the original idea, data generation and processing, MS preparation; P.G. (Corresponding author)—Conceived the original idea, data generation, processing and supervision of research, MS preparation; T.B.C.—Mg/Ca and δ¹¹B analysis, suggestions during MS preparation; M.S.—Statistical data processing, MS preparation; G.L.F.—Mg/Ca and δ¹¹B analysis, suggestions during MS preparation; R.M.—Provided the marine sedimentary core samples, suggestions during MS preparation.

Competing interests

The authors declare no competing interests.

Additional information

Supplementary Information The online version contains supplementary material available at <https://doi.org/10.1038/s41598-022-07774-4>.

Correspondence and requests for materials should be addressed to P.G.

Reprints and permissions information is available at www.nature.com/reprints.

Publisher's note Springer Nature remains neutral with regard to jurisdictional claims in published maps and institutional affiliations.



Open Access This article is licensed under a Creative Commons Attribution 4.0 International License, which permits use, sharing, adaptation, distribution and reproduction in any medium or format, as long as you give appropriate credit to the original author(s) and the source, provide a link to the Creative Commons licence, and indicate if changes were made. The images or other third party material in this article are included in the article's Creative Commons licence, unless indicated otherwise in a credit line to the material. If material is not included in the article's Creative Commons licence and your intended use is not permitted by statutory regulation or exceeds the permitted use, you will need to obtain permission directly from the copyright holder. To view a copy of this licence, visit <http://creativecommons.org/licenses/by/4.0/>.

© The Author(s) 2022